Room temperature Bi_2Te_3-based thermoelectric materials with high performance

Sahiba Bano[1,2] · Ashish Kumar[1,2] · Bal Govind[1,2] · Abdul Hanan Khan[1] · Anuradha Ashok[3] · D. K. Misra[1]

Abstract

Several off-stoichiometric compositions $Bi_{0.5}Sb_{1.5+x}Te_{3+\delta}$ ($x = 0.2$; $\delta = 0$, 0.12, 0.14) were deliberately synthesized to produce in-situ composites based on compositional engineering approach. The structural characterization of these materials employing XRD, SEM, and HR-TEM reveals the formation of in-situ-composites containing $Bi_{0.5}Sb_{1.5}Te_3$ as matrix phase and minor phases of either Sb rich or Te rich in different compositions. Thermoelectric properties of these $Bi_{0.5}Sb_{1.5+x}Te_{3+\delta}$ ($x = 0.2$; $\delta = 0$, 0.12, 0.14) composites were studied in a wide range of temperatures extending from room temperature to 500 K. The electronic transport of these composites exhibits p-type semiconducting materials. The lowest thermal conductivity of ~ 0.69 W/m K @310 K was observed for $Bi_{0.5}Sb_{1.7}Te_{3.12}$ composite, which was noted to be 14% reduced thermal conductivity when compared with that of the state-of-the-art $Bi_{0.5}Sb_{1.5}Te_3$ ($\kappa = 0.82$ W/m K) material. In addition to this, an enhanced power factor was also observed in $Bi_{0.5}Sb_{1.7}Te_{3.12}$ which is primarily due to increased electrical conductivity of these materials. This enhanced power factor of the composition of $Bi_{0.5}Sb_{1.7}Te_{3.12}$ coupled with reduced thermal conductivity yields to high ZT ~ 1.13 at nearly room temperature, making these materials viable for large scale applications.

1 Introduction

Thermoelectric (TE) technology enables solid-state cooling in refrigeration, air conditioning devices, and electronic devices by using small Peltier devices. For the use of TE devices at a large scale, improvement in the performance of thermoelectric materials is a prerequisite. TE performance of materials can be computed by a dimensionless quantity, called figure of merit (ZT). Figure of merit $(ZT) = (\alpha^2\sigma/\kappa)$ T where σ, α, and κ are the electrical conductivity, Seebeck coefficient, and total thermal conductivity respectively at the absolute temperature (T) [1]. High ZT can be optimized by decoupling of α, σ and κ as they have close interdependences. Solid solution alloying [2, 3], band engineering [4–7], mass fluctuation [8–11], nanostructuring/nanocomposites [12–14], doping [15–17], phonon-glass electron-crystal (PGEC) [18, 19] and defect engineering [20–22], have been implemented in order to enhance the value of ZT up to a certain extent.

Among all thermoelectric materials, Bi_2Te_3 is known as potential state-of-the-art thermoelectric materials exhibiting a typical narrow-gap semiconductor which has been extensively studied in regard to the investigation of thermoelectric properties. It exhibits rhombohedral structure (R−3 m, 166) consisting of three 2D quintuple layers of Te(2)–Bi–Te(1)–Bi–Te(2) along c axis. Ternary $Bi_{0.5}Sb_{1.5}Te_3$ alloy has been shown so far the best commercial p-type materials for low-temperature applications with peak of ZT 1.1 near 300 K [23].When it is prepared with conventional and different processing methods [24, 25] such as nanostructuring/nanocomposites results to a different value of ZT. The maximum value of ZT ~ 1.8 at 316 K was realized in composition $Bi_{0.4}Sb_{1.6}Te_3$ [26], through rapid solidification by melt-spinning. Thus, composition fluctuation in this ternary composition of $Bi_{0.5}Sb_{1.5}Te_3$ coupled with various powder metallurgical engineering has been found to increase ZT significantly [27–29]. Usually replacing Sb at

✉ D. K. Misra
misradk@nplindia.org

1 CSIR-National Physical Laboratory, Dr. K.S. Krishnan Marg, New Delhi 110012, India

2 AcSIR, Academy of Scientific & Innovative Research, Ghaziabad 201002, India

3 Department of Physics, PSG College of Technology NRIIC, PSG Institute of Advanced Studies Peelamedu, Coimbatore, Tamilnadu 641004, India

Bi site in $Bi_{0.5}Sb_{1.5}Te_3$, creates an atomic disorder of Bi-Sb which scatters heat-carrying high-frequency phonons to reduce the κ_L, thereby increased ZT has been observed [30]. Furthermore, recently nanostructuring/nanocomposites have been used as an efficient strategy to improve ZT via reducing thermal conductivity through grain boundary and interface boundary scattering of phonons in this family of compound [31, 32]. However, reasonably high ZT (≥ 2) in $Bi_{0.5}Sb_{1.5}Te_3$ bulk materials could not be get for its thermoelectric applications at large scale. Recently a remarkable finding by Kim et al. [33] producing a record high ZT ~ 1.85 at 320 K in 25wt% excess Te in $Bi_{0.5}Sb_{1.5}Te_3$ was observed, with the hope for the TE industry to develop TE module for cooling applications. However, it had further been noticed by other research group [34] that such high recorded ZT ~ 1.85 could not be reproduced. A synergetic optimization of power factor and a drastic reduction in thermal conductivity may lead to an expected result of achieving ZT ≥ 2. With this in mind, our critical observation of low σ ~ 400S/cm of $Bi_{0.5}Sb_{1.5}Te_3$ at room temperature [35] provides us an impetus to reasonably increase the electrical conductivity while either maintaining or increasing the Seebeck coefficient and reducing the thermal conductivity for realizing high yield of ZT.

Initially, we have taken excess Sb; $Bi_{0.5}Sb_{1.7}Te_3$ to increase hole concentration for high electrical conductivity. The increase in hole concentration can be realized because the difference in size and electronegativity between Sb–Te is much smaller than that of between Bi–Sb and Bi-Te, which makes Sb preferable to occupy the site as proposed by $\chi-r$ model [36]. Also, occupying Sb to Te site adds holes as Sb^{3+} gets replaced with Te^{2-}. Further, in order to optimize the Seebeck coefficient simultaneously with electrical conductivity in nominal composition $Bi_{0.5}Sb_{1.7}Te_3$, off-stoichiometric compositions $Bi_{0.5}Sb_{1.7}Te_{3+\delta}$ ($\delta = 0.12$, 0.14) with an excess of Te were synthesized. Interestingly, the composition $Bi_{0.5}Sb_{1.7}Te_3$ with an excess of Sb significantly increases electrical conductivity-parallel- i.e., $\sigma_{//}$ ~ 1200 S/cm at room temperature which is 200% larger than that of commercially reported $Bi_{0.5}Sb_{1.5}Te_3$ composition by Hao et al. [35]. However, α was found to be ~ 51% decreased ($\alpha_{//}$ ~ 110 μV/K) in comparison to that of $Bi_{0.5}Sb_{1.5}Te_3$($\alpha_{//}$ = 225 μV/K at 310 K) [35] but excess Sb and Te together in this work give synergistic effect to control over σ & α. Hence, increase in power factor along with reduced κ yielding a high ZT ~ 1.13 at room temperature.

2 Experimental details

2.1 Materials synthesis

Several stoichiometric compositions $Bi_{0.5}Sb_{1.5+x}Te_{3+\delta}$ ($x = 0.2$; $\delta = 0$, 0.12, 0.14) were measured by taking high purity

elements Sb powder (99%), Bi powder (99.9%), and Te powder (99%). The mixed powders were then sealed in a quartz tube in a vacuum at a pressure of 10^{-5} Torr. The sealed powders were further reacted in a furnace at 800 °C for 8 h and subsequently, water quenched at room temperature. The molten ingots were then grounded into fine powders for 15 min. These powder materials were then loaded into 12.7 mm diameter of graphite die and sintered by SPS at 673 K, pressure of 50 MPa with holding time of 3 min.

2.2 Phase and microstructure characterization

In order to investigate phase formation, powder X-ray diffractometer (PXRD, Model: Rigaku Mini Flex II) operated at 30 kV and 20 mA using Cu-Kα($\lambda = 1.54$ Å) has been performed on all composite materials. For microstructure investigation, scanning electron microscopy (SEM) and transmission electron microscopy (TEM) were used. Energy dispersive spectroscopy (EDS) was performed for composition and elemental analysis.

2.3 Thermoelectric property measurement

Laser Flash Analysis (Lineseis, LFA 1000) was performed on circular disc samples with a diameter of 12.7 mm and thickness of 1.5 mm for thermal diffusivity. For the estimation of specific heat, differential scanning calorimetry (DSC) (822e Mettler Toledo) is used. Further, thermal conductivity was estimated by using the relation $\kappa = d \times C_p \times \rho$, where d, C_p and ρ are diffusivity, specific heat, and density, respectively. The density (ρ) of all composites was found to be > 95% which was estimated using the Archimedes principle. The Seebeck coefficient and resistivity were measured by ULVAC, ZEM-3 from room temperature to 500 K.

3 Results and discussion

3.1 XRD analysis

Figure 1a shows the X-ray diffraction for samples $Bi_{0.5}Sb_{1.5+x}Te_{3+\delta}$ ($x = 0.2$; $\delta = 0$, 0.12, 0.14). All the peaks are primarily indexed with Bi_2Te_3 type rhombohedral structure together with a trace amount of either Sb or Te. It is envisaged from XRD (Fig. 1a) that the peak positions corresponding to a rhombohedral structure are found to be slightly shifted towards a low angle side indicating an increase in a and c. The Rietveld analysis was performed on all the samples to identify the phases and accurate estimation of lattice parameters and the Rietveld refinement corresponding to best-optimized $Bi_{0.5}Sb_{1.7}Te_{3.12}$ composition is presented in Fig. 1b. Variation of a and c parameters with increasing Te is presented in Fig. 1c. From Fig. 1c it
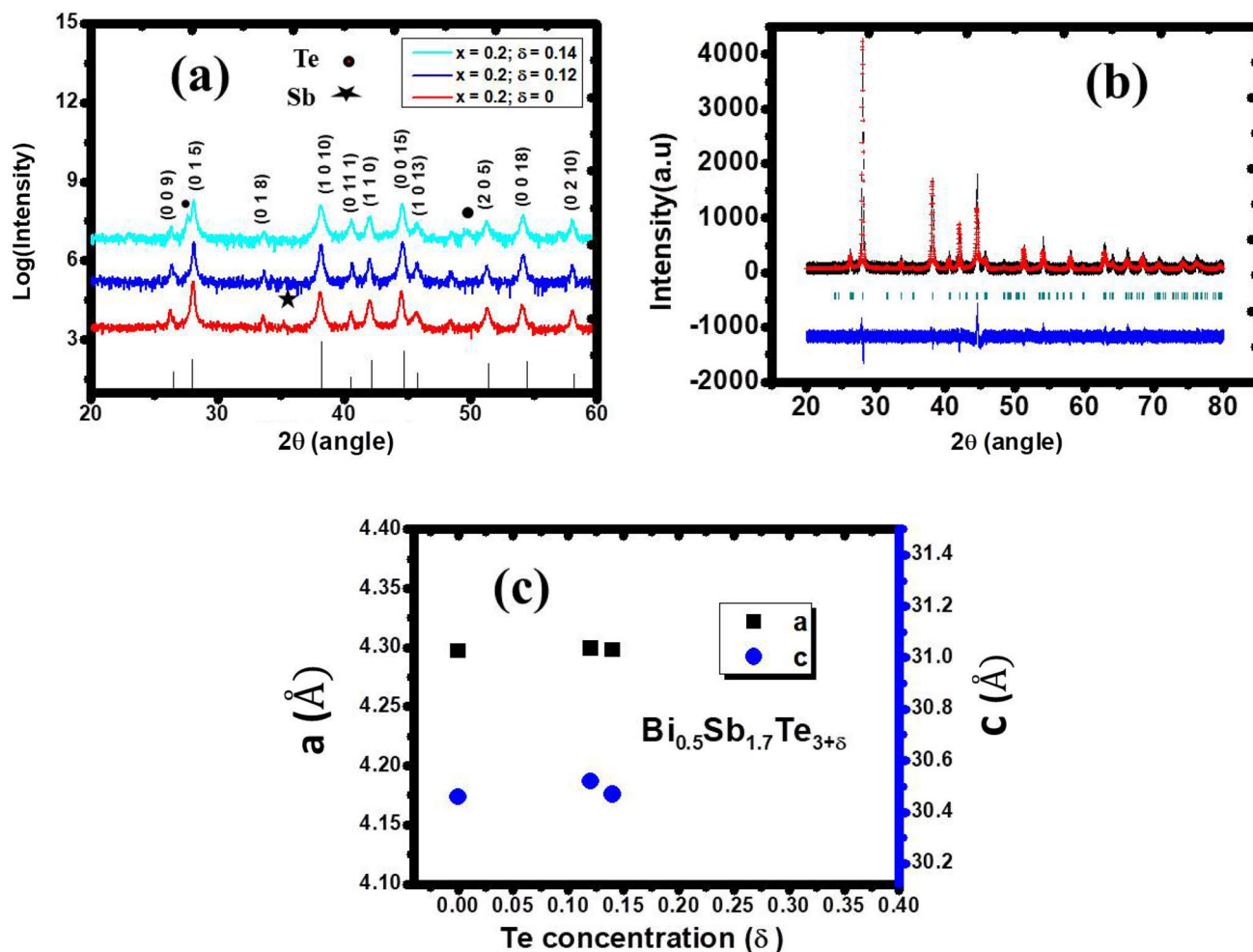
Fig. 1 **a** XRD pattern of samples of $Bi_{0.5}Sb_{1.5+x}Te_{3+\delta}$ ($x = 0.2$; $\delta = 0$, 0.12, 0.14). **b** Rietveld refinement of sample of $Bi_{0.5}Sb_{1.7}Te_{3.12}$ and **c** variation of **a** & **c** parameters with increasing Te concentration, obtained from Reitveld analysis using Fullprof software

is evident that the excess Te does not lead to the formation of a single solid solution phase as the trend does not follow the straights line of Vegard's law for solid solution phase formation. Evidently, increasing Te concentration increases the c-parameter with a slight change in 2Θ. It is important to point out that an increase in the c-parameter may be attributed to the Te occupied in the interstitial site between Te(1)–Te(1) Vander Waal gap.

In order to investigate the surface morphology and composition analysis, we have performed scanning electron microscopy (SEM), presented in the supporting information S1. SEM investigation reveals the formation of a composite phase containing a matrix phase of $Bi_{0.5}Sb_{1.5}Te_3$ and the minor phases of Sb and Te which is evident in supporting information (S1) on SEM investigation.

3.2 Transmission electron microscopy investigation

High-resolution of the best performing composition $Bi_{0.5}Sb_{1.7}Te_{3.12}$ was performed to examine more closely at the microstructure. A bright-field image obtained from the sample $Bi_{0.5}Sb_{1.7}Te_{3.12}$ is shown in Fig. 2a with grains size ranging from 100 to 200 nm. The enlarged view of the area (marked red circle in Fig. 2a) is shown in Fig. 2b. The high density of dislocation at the grain boundaries is found in this region. The enlarged view of the white box in Fig. 2b is presented in Fig. 2c. The d spacings are measured in two similar oriented grains marked as region 1 and region 2 (dotted circle). The measured d spacing in these two regions is noticed to be 3.01 Å and 3.15 Å. The difference in d spacing might have caused due to dislocation at the interface of both grains.
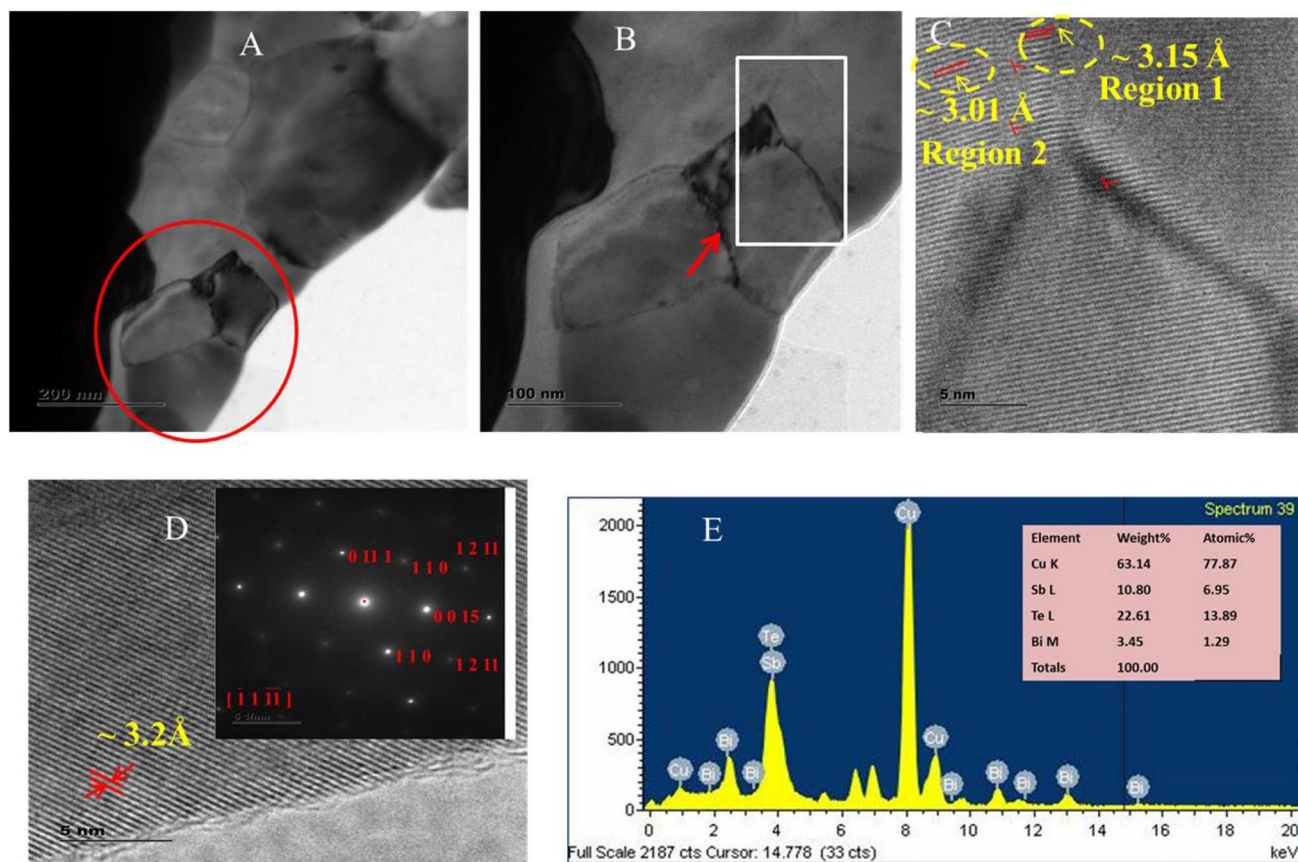
Fig. 2 a Bright field electron micrograph of the $Bi_{0.5}Sb_{1.7}Te_{3.12}$ composite displaying the dislocation embedded at the grain boundary (red circle); **b** enlarged view of circled region in (**a**); showing dislocation more clearly (red arrow) **(c)** HR-TEM image showing Misfit type of dislocation at interface; **d** HR-TEM image with inset of corresponding SAED confirming rhombohedral structure with a = 4.31 and c = 30.51 along zone axis [− 1 1 − 11] and **e** EDAX spectrum and quantification obtained from $Bi_{0.5}Sb_{1.7}Te_{3.12}$ revealing the composition close to the nominal composition (Color figure online)

Selected area electron diffraction (SAED) was recorded from the grains shown in Fig. 2d along [− 1 1 − 11] zone axis corresponding to $R − 3 m$ (166) structure. EDAX spectrum and quantification obtained from $Bi_{0.5}Sb_{1.7}Te_{3.12}$ are shown in Fig. 2e indicates all the elements are present and the presence of Cu was also noted which is appearing from Cu-grid. Quantification of EDAX analysis (inset Fig. 2e) reveals the composition close to the nominal composition with a slight variation in Bi concentration, which is noticed within the instrumental error.

3.3 Hall measurement

Carrier concentration is an important parameter to be analyzed to understand the thermoelectric properties. Table 1 represents the room temperature hall coefficient measurement. The carrier concentration was estimated by using $n_H = \frac{1}{R_H e}$ and mobility by $\sigma = ne\mu$ where μ = mobility, e = electron charge and σ = electrical conductivity and

Table 1 Hall measurement at room temperature of samples $Bi_{0.5}Sb_{1.5+x}Te_{3+\delta}$ ($x = 0.2$; $\delta = 0, 0.12, 0.14$)

Physical parameter	$Bi_{0.5}Sb_{1.7}Te_3$	$Bi_{0.5}Sb_{1.7}Te_{3.12}$	$Bi_{0.5}Sb_{1.7}Te_{3.14}$
Mobility (cm^2 $V^{-1} s^{-1}$)	456	309.6	307
n_H (per cm^3) $\times 10^{19}$	3.2	1.82	1.80
m^*/m_e	0.52	0.65	0.61

R_H = hall coefficient. For composition with excess Sb; $Bi_{0.5}Sb_{1.7}Te_3$, the carrier concentration $n_H = 3.2 \times 10^{19}/cm^3$ at room temperature, was observed which is about 52% larger than the commercially reported compound $Bi_{0.5}Sb_{1.5}Te_3$ ($n_H = 2.1 \times 10^{19}/cm^3$) [35]. Further, on increasing the Te content; $Bi_{0.5}Sb_{1.7}Te_{3.12}$ the carrier concentration decreases than the nominal composition $Bi_{0.5}Sb_{1.7}Te_3$ due to increase in Te_{Sb} antisite defects as shown in Table 1. However, surprisingly, excess Te; the $Bi_{05}Sb_{1.7}Te_{3\cdot12}$ exhibits the much higher mobility ($\mu =$

309.6 cm^2 V^{-1} s^{-1}) than the matrix Bi$_{0.5}$Sb$_{1.5}$Te$_3$ ($\mu = 120$ cm^2 V^{-1} s^{-1}) [35].

3.4 Electronic transport properties

Figure 3 depicts electrical conductivity (a, b) and Seebeck coefficient (c, d) measured parallel and perpendicular to pressing direction (α) of Bi$_{0.5}$Sb$_{1.5+x}$Te$_{3+\delta}$ ($x = 0.2$; $\delta = 0$, 0.12, 0.14) samples with increasing temperature. The results are also compared with that of commercially reported Bi$_{0.5}$Sb$_{1.5}$Te$_3$ [35] alloy. All samples exhibit a positive value of the Seebeck coefficient in the entire temperature range suggesting holes to be the majority charge carrier. Interestingly, the composition with excess Sb; Bi$_{0.5}$Sb$_{1.7}$Te$_3$, exhibits significantly increased electrical conductivity in both direction ($\sigma_{//} \sim 1200$ S/cm and $\sigma_{//} \sim 2400$ S/cm) at room temperature) which is 200% higher than that of commercially reported Bi$_{0.5}$Sb$_{1.5}$Te$_3$ ($\sigma_{//} \sim 400$ S/cm) [35] material in the parallel direction. This enhancement in electrical conductivity can be attributed to enhanced n$_H$ (3.2×10^{19} cm^{-3}) due to increased Sb$_{Te}$ antisite defects and also to increased mobility($\mu = 456$ cm^2 V^{-1} s^{-1}) due to reduced alloy scattering similar to other reports [37, 38]. It can be emphasized that the

scattering and mobility of carriers may be co-related based on the Mathiessien rule [39]. In normal doped semiconductors, there are two contributions namely acoustic (μ_{AC}) and the impurities (μ_I) scattering and the total mobility can be given by Matthiessen's rule,

$$\frac{1}{\mu} = \frac{1}{\mu_I} + \frac{1}{\mu_{AC}} \tag{1}$$

where μ_I and μ_{AC} is the mobility for ionized impurity scattering and acoustic phonon scattering, respectively.

In Bi$_2$Te$_3$-based materials, though both μ_I and μ_{AC} contribute to overall mobility. However, Bi$_2$Te$_3$-based materials involve lots of defects, so ionized impurity scattering plays an important role in overall mobility. Therefore, we have estimated the μ_I of ionized scattering as suggested by Li et al. [35]

$$\mu_I = \frac{64\sqrt{\pi}\varepsilon^2(2k_BT)^{3/2}}{N_Ie^3\sqrt{m_s^*}f(L_D)} \tag{2}$$

Herein, N_I is the ionized impurity concentration, m^* is a single valley effective mass given by $m^* = N_v^{2/3}m_s^*$ where N_v is valence band degeneracy, ε is the dielectric
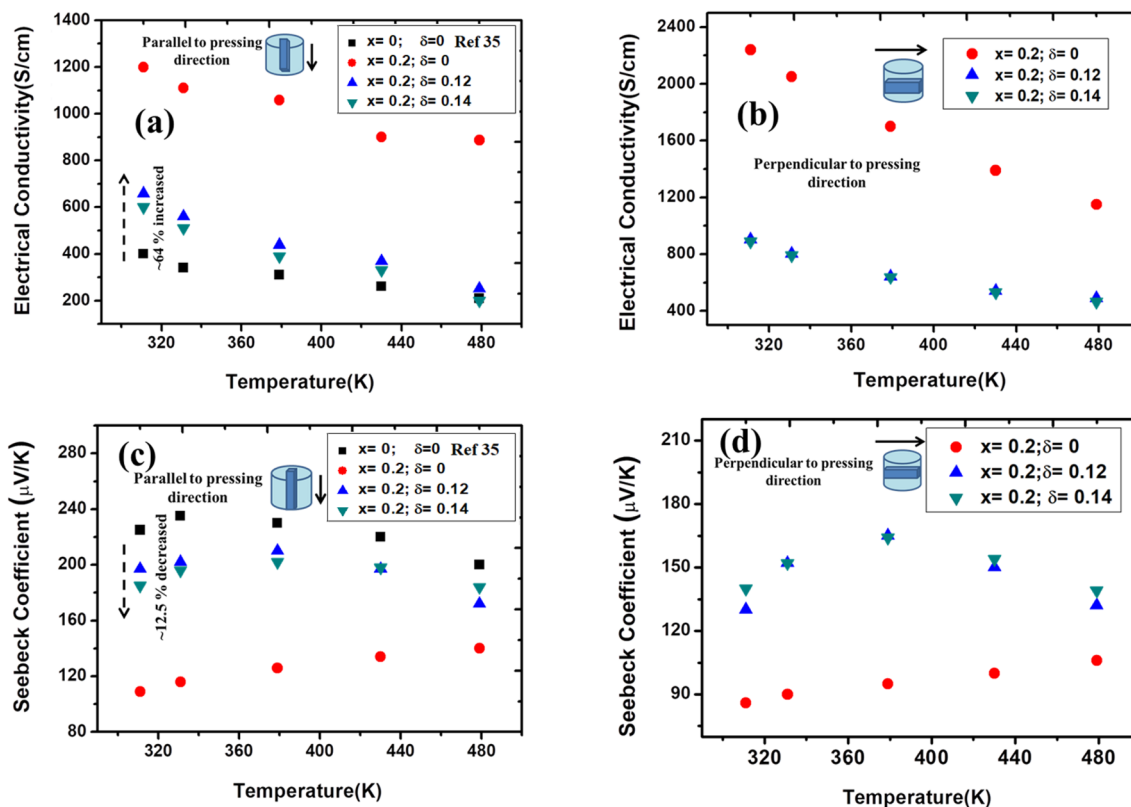

Fig. 3 a, b Temperature-dependent electrical conductivity and **c, d** Seebeck coefficient measured parallel and perpendicular to pressing direction of samples Bi$_{0.5}$Sb$_{1.5+x}$Te$_{3+\delta}$ ($x = 0.2$; $\delta = 0$, 0.12, 0.14)

constant. Dimensionless $f(L_D)$ parameter given above can be expressed as

$$f(L_D) = \ln\left(\frac{12m_s^* k_B T L_D^2}{\hbar^2} + 1\right) - \frac{12m_s^* k_B T L_D^2}{12m_s^* k_B T L_D^2 + \hbar^2} \quad (3)$$

where L_D, $\hbar$ is Debye screen length and reduced Planck constant respectively and L_D is defined as [35]:

$$L_D = \sqrt{\frac{\varepsilon k_B T}{ne^2}} \quad (4)$$

The estimated value of L_D by using the above relation for all our compositions is shown in Fig. 4. It is worth mentioning that short L_D corresponds to low coulomb potential around ionized impurity as suggested by Li et al. [35] which in turn gives a weak effect on carrier transport. Based on this fact, we can notice the lowest value of L_D in our nominal composition $Bi_{0.5}Sb_{1.7}Te_3$ which results to maximum mobility and this could be due to smaller coulomb potential similar to the earlier reports [35].

Further with increasing Te concentration, the σ decreases in the entire measured temperature as compared to $Bi_{0.5}Sb_{1.7}Te_3$ in both directions. The composition with excess Te; $Bi_{0.5}Sb_{1.7}Te_{3.12}$ exhibits the electrical conductivity ($\sigma_{//}$) measured parallel to the pressing direction to be of ~ 658 S/cm which is 64% larger than the commercially reported $Bi_{0.5}Sb_{1.5}Te_3$ compound. On increasing the Te concentration further; for instance in the case of $Bi_{0.5}Sb_{1.7}Te_{3.14}$ the electrical conductivity was noted to be almost the same as in the case of $Bi_{0.5}Sb_{1.7}Te_{3.12}$ for both directions. The Seebeck coefficient measured in parallel and perpendicular to the pressing direction of $Bi_{0.5}Sb_{1.7}Te_3$ in the entire temperature range is presented in Fig. 3c, d. On increasing the Te concentration; for $Bi_{0.5}Sb_{1.7}Te_{3.12}$ and $Bi_{0.5}Sb_{1.7}Te_{3.14}$, the Seebeck coefficient

is observed to be increased in parallel to pressing direction as well as in perpendicular to pressing direction [Fig. 3c, d] in comparison to that of nominal composition $Bi_{0.5}Sb_{1.7}Te_3$ [35]. For instance, the Seebeck coefficient of best-optimized composition $Bi_{0.5}Sb_{1.7}Te_{3.12}$ exhibits $\alpha_{//} \sim 195$ µV/K at room temperature which is much larger than $\alpha_{//} \sim 110$ µV/K for nominal composition $Bi_{0.5}Sb_{1.7}Te_3$.

The rationale behind the increasing α on increasing the Te concentration in $Bi_{0.5}Sb_{1.7}Te_{3.12}$ and $Bi_{0.5}Sb_{1.7}Te_{3.14}$ as compared to the nominal composition $Bi_{0.5}Sb_{1.7}Te_3$ of present work can be explained through a model which was proposed by Nolas et al. [40] for the Seebeck coefficient. This model relates the scattering factor with reduced Fermi energy which can be given as

$$\alpha = \frac{\pi^2 K_B}{3e}\left(r + \frac{2}{3}\right)\left(\frac{1}{\xi}\right)$$

where, K_B, ξ, r is the Boltzmann constant, reduced Fermi energy and scattering factor, respectively. The carrier concentration is related to reduced Fermi energy and for samples $Bi_{0.5}Sb_{1.7}Te_{3.12}$ and $Bi_{0.5}Sb_{1.7}Te_{3.14}$, the low value of carrier concentration corresponds to reduced Fermi energy resulting in a high value of Seebeck coefficient as compared to the nominal composition $Bi_{0.5}Sb_{1.7}Te_3$ in the present study.

In order to further understand the transport behavior of the present composites, we have plotted the Seebeck coefficient with carrier density, i.e., Pisarenko plot, obtained from a simple electron transport model, given below:

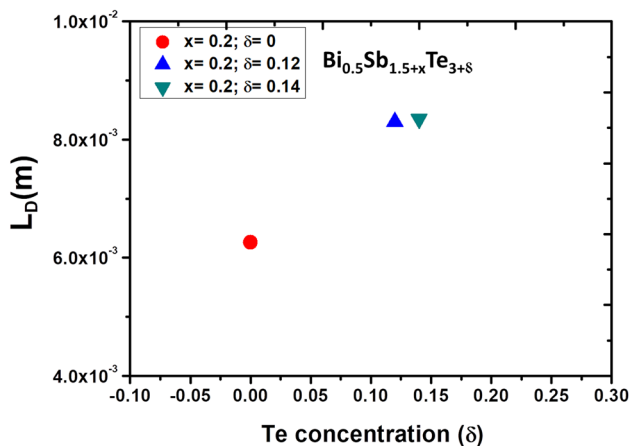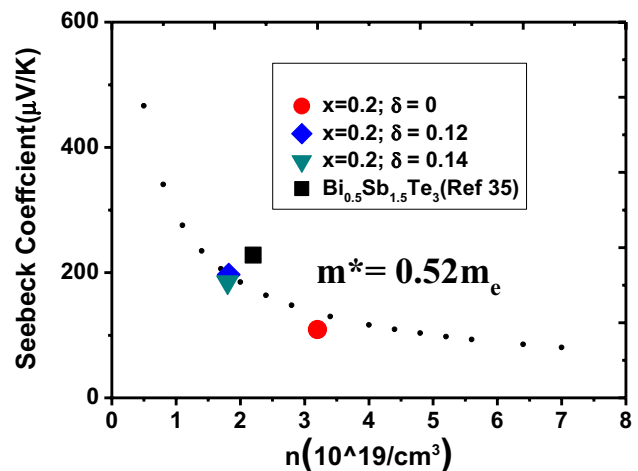$$\alpha = \left(\frac{8\pi^2 k_B^2}{3qh^2}\right)m^* T\left(\frac{\pi}{3n}\right)^{\frac{2}{3}}$$

Fig. 4 Estimated Debye screen length (L_D) with Te concentration in $Bi_{0.5}Sb_{1.5+x}Te_{3+\delta}$ ($x = 0.2$; $\delta = 0$, 0.12, 0.14)

Fig. 5 Pisarenko Plot at 310 K showing Seebeck dependences on hole concentration for all samples $Bi_{0.5}Sb_{1.5+x}Te_{3+\delta}$ ($x = 0.2$; $\delta = 0$, 0.12, 0.14)

The Fig. 5 shows the Pisarenko plot for compositions $Bi_{0.5}Sb_{1.5+x}Te_{3+\delta}$ ($x = 0.2$; $\delta = 0, 0.12, 0.14$). The Seebeck coefficient for a given temperature is explained using a single parabolic band (SPB) based on effective mass (m^*) due to single charge carriers. The density of states effective mass (m^*) was estimated from the Seebeck coefficient and carrier concentration by using the above equation. The estimated effective mass for all samples is given in Table 1. We observed from the Pisarenko plot that, the value of m^* for composites does not lie on the single parabolic curve indicating that the composites exhibit different effective mass and hence they do not follow the SPB. Thus, excess Sb and Te significantly alter the electronic band structure close in proximity of the Fermi level and hence the transport properties are significantly modified.

Figure 6 shows the power factor measured parallel to pressing direction and perpendicular to pressing direction (PF = $\alpha^2\sigma$) of $Bi_{0.5}Sb_{1.5+x}Te_{3+\delta}$ ($x = 0.2$; $\delta = 0, 0.2, 0.4$) samples with increasing temperature. The parallel power factor ($PF_{//}$) of present derived compositions $Bi_{0.5}Sb_{1.5+x}Te_{3+\delta}$ ($x = 0.2$; $\delta = 0, 0.2, 0.4$) is observed to be significantly increased than that of commercially reported $Bi_{0.5}Sb_{1.5}Te_3$ [35]. The enhancement in power factor in the entire temperature range is primarily due to increased electrical conductivity. Interestingly, at room temperature, the $PF_{//}$ for best-optimized composition $Bi_{0.5}Sb_{1.7}Te_{3.12}$ is 25.5×10^{-4} W/m K^2 which is 16% larger than that of the commercially reported $Bi_{0.5}Sb_{1.5}Te_3$ compound ($PF_{//} \sim 22 \times 10^{-4}$ W/m K^2) [35].

3.5 Thermal transport properties

The thermal conductivity (κ) is another important property to be studied for the estimation of ZT. Figure 7a, b represents the temperature-dependent thermal conductivity of $Bi_{0.5}Sb_{1.5+x}Te_{3+\delta}$ ($x = 0.2$; $\delta = 0, 0.2, 0.4$) alloys measured parallel as well as perpendicular to pressing direction. We have also compared the thermal conductivity measured in the parallel direction ($\kappa_{//}$) with the reported values measured in the parallel direction of commercially $Bi_{0.5}Sb_{1.5}Te_3$ [35] material. The total thermal conductivity for all samples increases with increasing temperature in both directions which is consistent with temperature dependence electrical conductivity and Seebeck coefficient. Interestingly, the parallel thermal conductivity of optimized composition $Bi_{0.5}Sb_{1.7}Te_{3.12}$ exhibits much reduced thermal conductivity compared to that of commercially reported $Bi_{0.5}Sb_{1.5}Te_3$ [35] and lowest value of $\kappa_{//}$ found to be 0.7 W/m K at 311 K for best performing composition $Bi_{0.5}Sb_{1.7}Te_{3.12}$ which is 14% smaller than that of commercial composition $Bi_{0.5}Sb_{1.5}Te_3$($\kappa_{//} \sim 0.8$ W/m K) [35]. The total thermal conductivity has three contributions i.e., lattice thermal conductivity (κ_L), electronic thermal conductivity (κ_e) and bipolar thermal conductivity ($\kappa_{bipolar}$). For Bi_2Te_3-based TE materials, an inverse relationship between κ_L and $T(\kappa_L = aT^{-1} + b)$ above the Debye temperature (160 K) follows the Umklapp scattering mechanism [41]. Here we have estimated the lattice thermal conductivity κ_L (by subtracting the electronic thermal conductivity $\kappa_e = L\sigma T$ where L is the Lorentz number, here $L = 1.6 \times 10^{-8}/V^2K^2$ [33] is considered in the present study) from total thermal conductivity over the temperature in which intrinsic excitation is neglected. Then, we calculated the κ_L for higher temperature according to the relation $\kappa_L = aT^{-1} + b$ and $\kappa_{bipolar}$ using equation $\kappa_{total} = \kappa_L + \kappa_{e+}\kappa_{Bipolar}$ which are shown in Fig. 7c–f. Interestingly, with increasing the Te concentration the value of lattice thermal conductivity decreases and reached the lowest parallel lattice thermal conductivity ~ 0.40 W/ m K for $Bi_{0.5}Sb_{1.7}Te_{3.12}$, at room temperature which is about

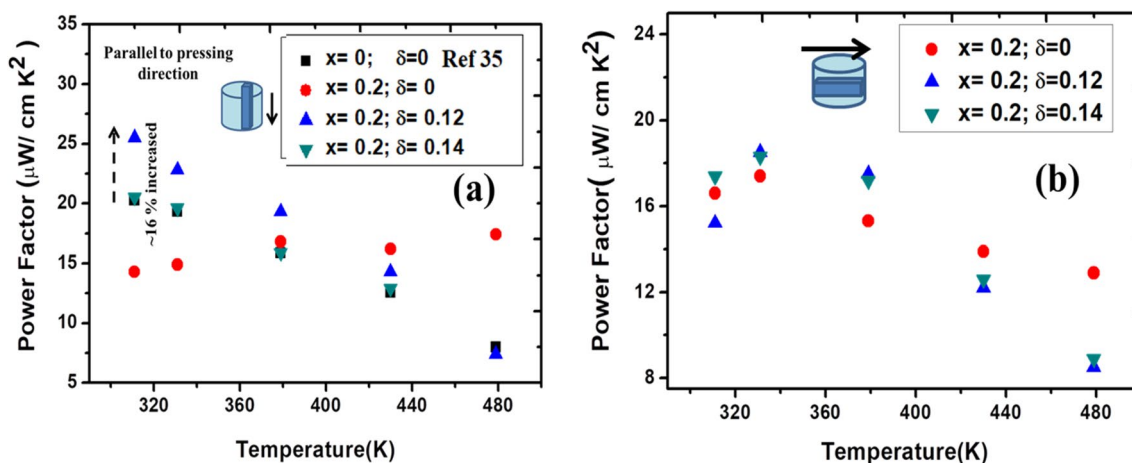**Fig. 6** Temperature dependence of Power factor measured parallel and perpendicular to pressing direction of samples $Bi_{0.5}Sb_{1.5+x}Te_{3+\delta}$ ($x = 0.2$; $\delta = 0, 0.12, 0.14$)

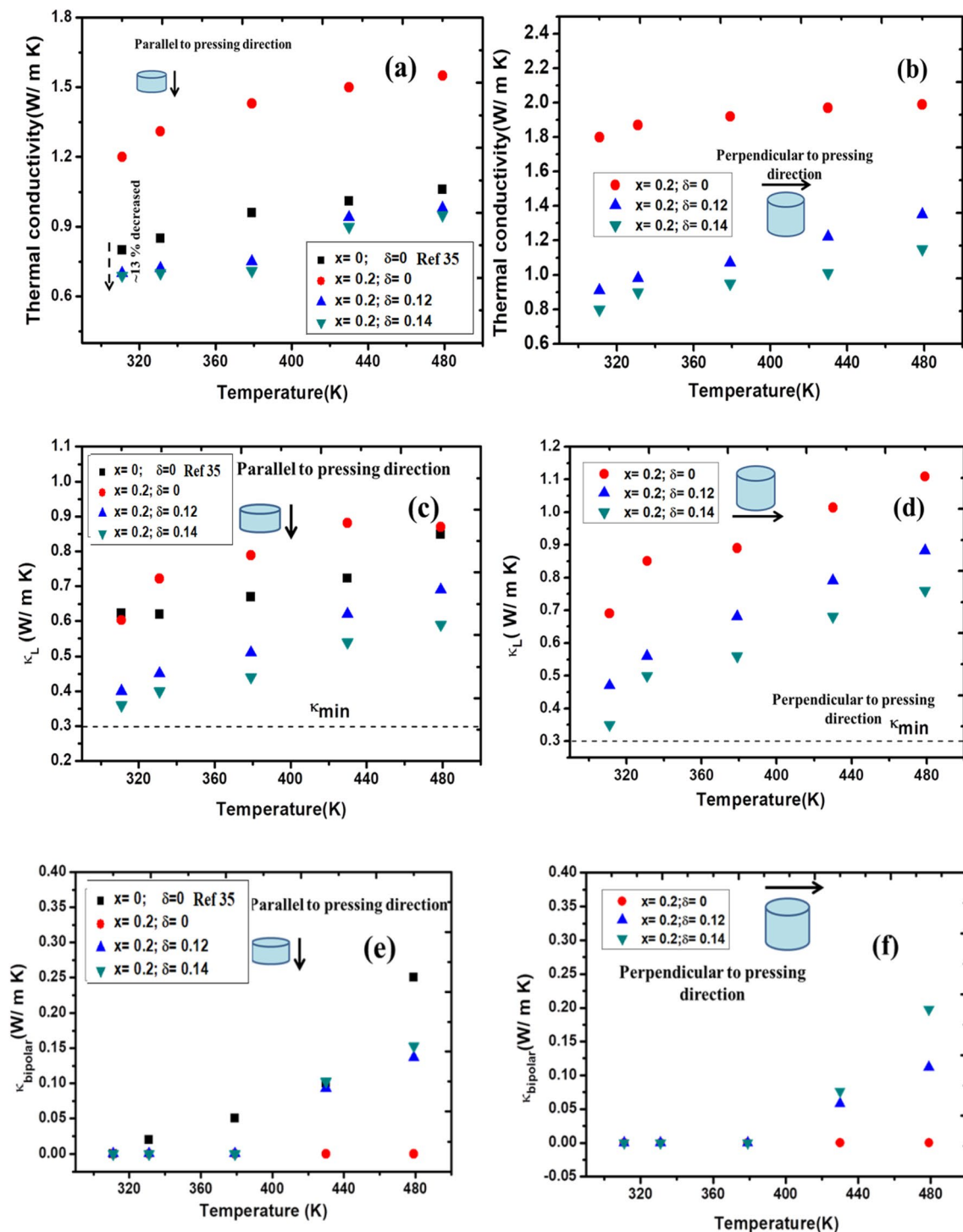**Fig. 7** The temperature dependence of parallel and perpendicular, **a**, **b** total thermal conductivity; **c**, **d** lattice thermal and **e**, **f** bipolar thermal conductivity of samples $Bi_{0.5}Sb_{1.5+x}Te_{3+\delta}$ ($x = 0.2$; $\delta = 0, 0.12, 0.14$)

33% lower than that of commercially reported compound $Bi_{0.5}Sb_{1.5}Te_3$ ($\kappa_{//} = 0.6$ W/m K at 300 K). The reduced lattice thermal conductivity in this alloy is attributed to the scattering of phonons from grain boundaries, defects, dislocations and interfaces produced by excess Te.

3.6 Thermoelectric figure of merit (ZT)

The estimated value of parallel and perpendicular ZT are displayed in Fig. 8a, b. As shown in Fig. 8a, the highest $ZT_{//} \sim 1.13$ near room temperature was achieved for
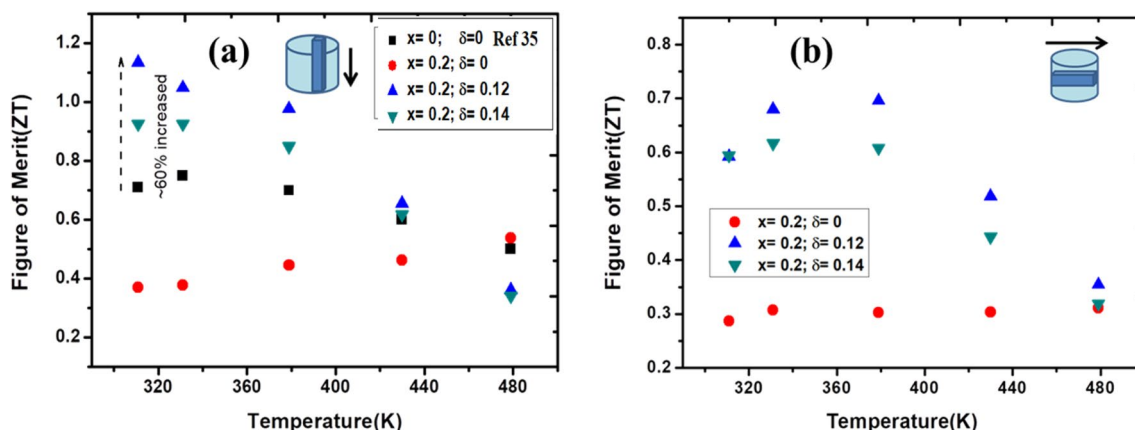
Fig. 8 The temperature-dependent **a** parallel ZT and **b** perpendicular ZT of $Bi_{0.5}Sb_{1.5+x}Te_{3+\delta}$ ($x = 0.2$; $\delta = 0, 0.12, 0.14$)

$Bi_{0.5}Sb_{1.7}Te_{3.12}$ which is about 60% larger compared to the commercially reported $Bi_{0.5}Sb_{1.5}Te_3$ ($ZT_{//} = 0.71$ at 310 K) [35]. Such high ZT ~ 1.13 at room temperature makes it feasible to develop thermoelectric devices because maintaining the room temperature gradient between hot and cold end is easier than maintaining the temperature gradient more than 100 °C in the commercially available thermoelectric materials.

This favorable situation might have occurred due to unusual electronic transport due to excess Te. Further, unusual increase of m^* and unusual decrease in μ in the present work derives a new measuring parameter, ie. quality factor (B) [42] which governs the thermoelectric figure of merit. The quality factor basically originates from the parameters associated with the electronic and lattice structure, namely, m^*, μ, and κ_L and defined by

$$B = \frac{\mu m_*^{1.5} T^{2.5}}{\kappa_L}$$

where μ κ_L and m^* is the carrier mobility, lattice thermal conductivity, and effective mass, respectively. The estimated quality factor for all compositions is plotted with their corresponding ZT. Evidently, the increasing quality factor results in increasing the ZT (Fig. 9) which is consistent with the model [42].

3.7 Thermoelectric compatibility factor

Thermoelectric compatibility has been computed by Snyder et al. [43] using a relation $s = \frac{\sqrt{(1+ZT)} - 1}{\alpha T}$ to find the applicability of a segment of thermoelectric materials with other thermoelectric segment for better efficiency. Herein, we have also estimated the compatibility factor(s) for $Bi_{0.5}Sb_{1.5+x}Te_{3+\delta}$ ($x = 0.2$; $\delta = 0, 0.12, 0.14$) (Fig. 10) to have an understanding for the suitability of these materials to be
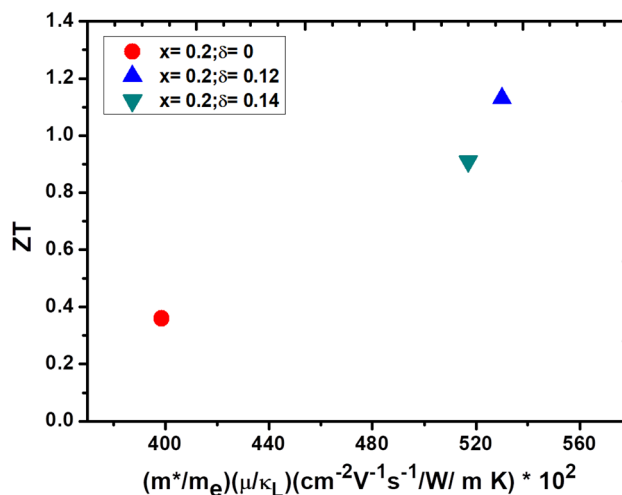

Fig. 9 The graph of $ZT_{//}$ verses $(m^*/m_e)/(\mu/\kappa_L)$ for samples $Bi_{0.5}Sb_{1.5+x}Te_{3+\delta}$ ($x = 0.2$; $\delta = 0, 0.12,$ and 0.14)
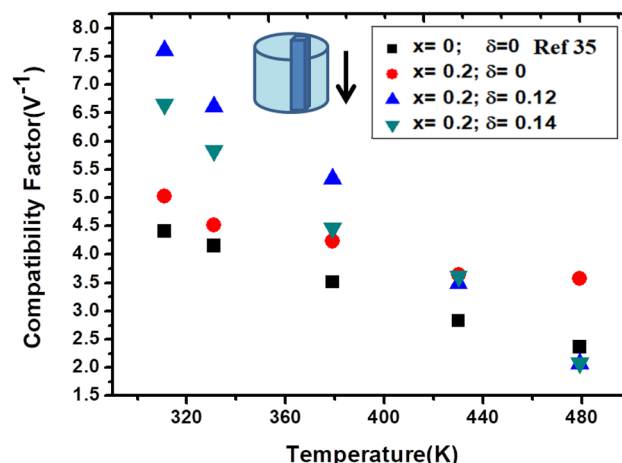

Fig. 10 Compatibility factor (s) for $Bi_{0.5}Sb_{1.5+x}Te_{3+\delta}$ ($x = 0.2$; $\delta = 0$, 0.12, 0.14) at different temperature

deployed with another counterpart in making a thermoelectric couple for maximum performance of the device. It can be noticed that the compatibility factor of $Bi_{0.5}Sb_{1.7}Te_{3.12}$ is 7.61 V^{-1} at 310 K which is favorable as suggested by Snyder et al. [43] for maximum efficiency [44].

4 Conclusion

Novel in-situ composites have been synthesized by varying stoichiometric $Bi_{0.5}Sb_{1.5+x}Te_{3+\delta}$ ($x = 0.2$; $\delta = 0$, 0.12, 0.14) compositions based on compositional engineering approach. The addition of an excess amount of Sb in a nominal composition $Bi_{0.5}Sb_{1.7}Te_3$ primarily brings the system of significantly increased electrical conductivity. Further, excess Te incorporation in such derived $Bi_{0.5}Sb_{1.7}Te_3$ composition leads to synergistically modify the Seebeck coefficient and thermal conductivity. The optimum combination of Sb and Te in present compositions $Bi_{0.5}Sb_{1.5+x}Te_{3+\delta}$ ($x = 0.2$; $\delta = 0$, 0.12, 0.14) leads to modify the materials into composites with unusual electronic transport behavior favorable to high ZT. A remarkably high ZT ~ 1.13 at room temperature was optimized in the best performing composition $Bi_{0.5}Sb_{1.7}Te_{3.12}$. The enhanced ZT is attributed due to synergistically optimized large power factor (25.5×10^{-4} W/m K^2) and reduced thermal conductivity (0.69 W/m K at 311 K). This approach of compositional modification to synthesize in-situ composites provides excellent means of twinning the thermoelectric parameters. Further, it may be thought that controlled compositional engineering in Bi_2Te_3-based thermoelectric materials can lead to a result even higher ZT than ZT ~ 1.13 at room temperature. We strongly believe that such ZT materials at room temperature will enable them to be deployed for thermoelectric devices for power generation/cooling on a large scale.

Compliance with ethical standards

Conflict of interest The authors declare that they have no known competing financial interests or personal relationships that could have appeared to influence the work reported in this paper.

References

1. G.J. Snyder, E.S. Toberer, Complex thermoelectric materials. Nat. Mater. **7**, 105–114 (2008). https://doi.org/10.1038/nmat2090
2. M.E. Anderson, S.S.N. Bharadwaya, R.E. Schaak, Modified polyol synthesis of bulk-scale nanostructured bismuth antimony telluride. J. Mater. Chem. **20**, 8362–8367 (2010). https://doi.org/10.1039/C0JM01424A
3. S. Dutta, V. Shubha, T.G. Ramesh, Reduction in thermal conductivity of Bi-Te alloys through grain refinement method. Bull. Mater. Sci. **36**, 853–857 (2013). https://doi.org/10.1007/s12034-013-0532-6
4. Y. Zheng, Q. Zhang, X. Su, H. Xie, S. Shu, T. Chen, G. Tan, Y. Yan, X. Tang, C. Uher, Mechanically robust BiSbTe alloys with superior thermoelectric performance: a case study of stable hierarchical nanostructured thermoelectric materials. Adv. Energy Mater. **5**, 1401391 (2015)
5. Y. Zhang, X. Jia, H. Sun, B. Sun, B. Liu, H. Liu, L. Kong, H. Ma, Enhanced thermoelectric performance of nanostructured CNTs/BiSbTe bulk composite from rapid pressure-quenching induced multi-scale microstructure. J. Mater. **2**, 316–323 (2016)
6. Y. Pei, X. Shi, A. LaLonde, H. Wang, L. Chen, G.J. Snyder, Convergence of electronic bands for high performance bulk thermoelectrics. Nature **473**, 66–69 (2011). https://doi.org/10.1038/nature09996s
7. M. Cho, *Two-dimensional optical spectroscopy* (CRC Press, Boca Raton, 2009). https://doi.org/10.1201/9781420084306
8. C. Fu, S. Bai, Y. Liu, Y. Tang, L. Chen, X. Zhao, T. Zhu, Realizing high figure of merit in heavy-band p-type half-Heusler thermoelectric materials. Nat. Commun. **6**, 8144 (2015)
9. Q. Zhang, J. He, T.J. Zhu, S.N. Zhang, X.B. Zhao, T.M. Tritt, High figures of merit and natural nanostructures in Mg 2 Si 0.4 Sn 0.6 based thermoelectric materials. Appl. Phys. Lett. **93**, 102109 (2008)
10. M. Guan, K. Zhao, P. Qiu, D. Ren, X. Shi, L. Chen, Enhanced thermoelectric performance of quaternary $Cu_{2-2X}Ag_{2X}Se_{1-X}SX$ Liquid-like Chalcogenides. ACS Appl. Mater. Interfaces **11**, 13433–13440 (2019)
11. N.S. Chauhan, S. Bathula, B. Gahtori, Y.V. Kolen'ko, A. Dhar, Enhanced thermoelectric performance in Hf-Free p-type (Ti, Zr) CoSb half-heusler alloys. J. Electron. Mater. **48**, 6700–6709 (2019)
12. Y. Du, K.F. Cai, S. Chen, P. Cizek, T. Lin, Facile preparation and thermoelectric properties of Bi2Te3 based alloy nanosheet/PEDOT: PSS composite films. ACS Appl. Mater. Interfaces **6**, 5735–5743 (2014)
13. X.B. Zhao, X.H. Ji, Y.H. Zhang, T.J. Zhu, J.P. Tu, X.B. Zhang, Bismuth telluride nanotubes and the effects on the thermoelectric properties of nanotube-containing nanocomposites. Appl. Phys. Lett. **86**, 62111 (2005)
14. W. Xie, J. He, H.J. Kang, X. Tang, S. Zhu, M. Laver, S. Wang, J.R.D. Copley, C.M. Brown, Q. Zhang, Identifying the specific nanostructures responsible for the high thermoelectric performance of $(Bi, Sb)_2Te_3$ nanocomposites. Nano Lett. **10**, 3283–3289 (2010)
15. B. Chen, J. Li, M. Wu, L. Hu, F. Liu, W. Ao, Y. Li, H. Xie, C. Zhang, Simultaneous enhancement of the thermoelectric and mechanical performance in one-step sintered n-type Bi2Te3-based alloys via a facile MgB2 doping strategy. ACS Appl. Mater. Interfaces **11**, 45746–45754 (2019)
16. M.U. Muzaffar, B. Zhu, Q. Yang, Y. Zhou, S. Zhang, Z. Zhang, J. He, Suppressing bipolar effect to broadening the optimum range of thermoelectric performance for p-type bismuth telluride–based alloys via calcium doping. Mater. Today Phys. **9**, 100130 (2019)
17. Z. Wang, Y. Yokoyama, T. Onda, Y. Adachi, Z. Chen, Improved thermoelectric properties of hot-extruded Bi–Te–Se bulk materials with Cu doping and property predictions via machine learning. Adv. Electron. Mater. **5**, 1900079 (2019)
18. P.-C. Gharleghi, F.-H. Hung, C.-J. Lin, Liu, Enhanced ZT of In x Co_4Sb_{12}–InSb nanocomposites fabricated by hydrothermal synthesis combined with solid-vapor reaction: a signature of

phonon-glass and electron-crystal materials. ACS Appl. Mater. Interfaces **8**, 35123–35131 (2016)

19. T. Zhu, Y. Liu, C. Fu, J.P. Heremans, J.G. Snyder, X. Zhao, Compromise and synergy in high-efficiency thermoelectric materials. Adv. Mater. **29**, 1605884 (2017)

20. Q. Zhang, B. Gu, Y. Wu, T. Zhu, T. Fang, Y. Yang, J. Liu, B. Ye, X. Zhao, Evolution of the intrinsic point defects in bismuth telluride-based thermoelectric materials. ACS Appl. Mater. Interfaces **11**, 41424–41431 (2019)

21. K.T. Kim, T.S. Min, S.-D. Kim, E.-A. Choi, D.W. Kim, S.-Y. Choi, Strain-mediated point defects in thermoelectric p-type bismuth telluride polycrystalline. Nano Energy **55**, 486–493 (2019)

22. J. Li, C. Zhang, Y. Feng, C. Zhang, Y. Li, L. Hu, W. Ao, F. Liu, Effects on phase transition and thermoelectric properties in the Pb-doped GeTe-Bi2Te3 alloys with thermal annealing. J. Alloys Compd. **808**, 151747 (2019)

23. W.M. Yim, E.V. Fitzke, F.D. Rosi, Thermoelectric properties of Bi2Te3-Sb2Te3-Sb2Se3 pseudo-ternary alloys in the temperature range 77 to 300°K. J. Mater. Sci. **1**, 52–65 (1966). https://doi.org/10.1007/BF00549720

24. D.M. Rowe, *CRC handbook of thermoelectrics* (CRC Press, Boca Raton, 2018)

25. B. Poudel, Q. Hao, Y. Ma, Y. Lan, A. Minnich, B. Yu, X. Yan, D. Wang, A. Muto, D. Vashaee, X. Chen, J. Liu, M.S. Dresselhaus, G. Chen, Z. Ren, High-thermoelectric performance of nanostructured bismuth antimony telluride bulk alloys. Science **320**, 634–638 (2008). https://doi.org/10.1126/science.1156446

26. S. Fan, J. Zhao, J. Guo, Q. Yan, J. Ma, H.H. Hng, p-type Bi 0.4 Sb 1.6 Te 3 nanocomposites with enhanced figure of merit. Appl. Phys. Lett. **96**, 182104 (2010)

27. S.V. Ovsyannikov, N.V. Morozova, I.V. Korobeinikov, L.N. Lukyanova, A.Y. Manakov, A.Y. Likhacheva, A.I. Ancharov, A.P. Vokhmyanin, I.F. Berger, O.A. Usov, V.A. Kutasov, V.A. Kulbachinskii, T. Okada, V.V. Shchennikov, Enhanced power factor and high-pressure effects in (Bi, Sb)$_2$(Te, Se)$_3$ thermoelectrics. Appl. Phys. Lett. **106**, 3–8 (2015). https://doi.org/10.1063/1.4916947

28. Y.Q. Cao, X.B. Zhao, T.J. Zhu, X.B. Zhang, J.P. Tu, Syntheses and thermoelectric properties of Bi2 Te3 Sb2 Te3 bulk nanocomposites with laminated nanostructure. Appl. Phys. Lett. (2008). https://doi.org/10.1063/1.2900960

29. J.J. Shen, T.J. Zhu, X.B. Zhao, S.N. Zhang, S.H. Yang, Z.Z. Yin, Recrystallization induced in situ nanostructures in bulk bismuth antimony tellurides: a simple top down route and improved thermoelectric properties. Energy Environ. Sci. (2010). https://doi.org/10.1039/c0ee00012d

30. H.J. Goldsmid, *Electronic refrigeration* (Pion, London, 1986), pp. 57–87

31. B.H. Poudel, Q. Ma, Y. Lan, Y. Minnich, A. Yu, B. Yan, X. Wang, D. Muto, A. Vashaee, D. Chen, X. Liu, J. Dresselhaus, M.S. Chen, and Ren Z, High-thermoelectric performance of nanostructured bismuth antimony telluride bulk alloys. Science **320**, 634–638 (2008)

32. Y. Ma, Q. Hao, B. Poudel, Y. Lan, B. Yu, D. Wang, G. Chen, Z. Ren, Enhanced thermoelectric figure-of-merit in p-type nanostructured bismuth antimony tellurium alloys made from elemental chunks. Nano Lett. **8**, 2580–2584 (2008)

33. S. Il Kim, K.H. Lee, H.A. Mun, H.S. Kim, S.W. Hwang, J.W. Roh, D.J. Yang, W.H. Shin, X.S. Li, Y.H. Lee, G.J. Snyder, S.W. Kim, Dense dislocation arrays embedded in grain boundaries for high-performance bulk thermoelectrics. Science **348**, 109–114 (2015). https://doi.org/10.1126/science.aaa4166

34. R. Deng, X. Su, Z. Zheng, W. Liu, Y. Yan, Q. Zhang, V.P. Dravid, C. Uher, M.G. Kanatzidis, X. Tang, Dense dislocation arrays at grain boundaries. Sci. Adv. **4**, eaar5606 (2018)

35. P. Lu, L. Chen, H. Chen, F. Hao, D. Ren, Q. Song, P. Qiu, X. Shi, Roles of Cu in the enhanced thermoelectric properties in Bi0.5Sb1.5Te3. Materials (Basel). **10**, 251 (2017). https://doi.org/10.3390/ma10030251

36. Z. Xu, H. Wu, T. Zhu, C. Fu, X. Liu, L. Hu, J. He, J. He, X. Zhao, Attaining high mid-temperature performance in (Bi, Sb)$_2$Te$_3$ thermoelectric materials via synergistic optimization. NPG Asia Mater. **8**, e302 (2016)

37. W.M. Yim, F.D. Rosi, Compound tellurides and their alloys for peltier cooling—a review. Solid State Electron. **15**, 1121–1140 (1972)

38. W.M. Yim, E.V. Fitzke, F.D. Rosi, Thermoelectric properties of Bi$_2$Te$_3$-Sb$_2$Te$_3$-Sb$_2$Se$_3$ pseudo-ternary alloys in the temperature range 77 to 300 K. J. Mater. Sci. **1**, 52–65 (1966)

39. E.S. Zevalkink, W.G. Toberer, E. Zeier, G.J. Flage-Larsen, Snyder, Ca3AlSb3: an inexpensive, non-toxic thermoelectric material for waste heat recovery. Energy Environ. Sci. **4**, 510–518 (2011). https://doi.org/10.1039/C0EE00517G

40. G.S. Nolas, J. Sharp, J. Goldsmid, *Thermoelectrics: basic principles and new materials developments* (Springer, New York, 2013)

41. F. Hao, P. Qiu, Y. Tang, S. Bai, T. Xing, H.-S. Chu, Q. Zhang, P. Lu, T. Zhang, D. Ren, High efficiency Bi$_2$ Te$_3$-based materials and devices for thermoelectric power generation between 100 and 300 C. Energy Environ. Sci. **9**, 3120–3127 (2016)

42. G.J. Snyder, T.S. Ursell, Thermoelectric efficiency and compatibility. Phys. Rev. Lett. **91**, 148301 (2003)

43. G.J. Snyder, Application of the compatibility factor to the design of segmented and cascaded thermoelectric generators. Appl. Phys. Lett. **84**, 2436–2438 (2004)

44. E. Maciá, Compatibility factor of segmented thermoelectric generators based on quasicrystalline alloys. Phys. Rev. B **70**, 100201 (2004)